Chapter 4

Numerical Simulations

To account for the search in each algorithm, the optimization tool fminsearch in MATLAB 6.5 is used without any specification on its option.

In the numerical complexity experiments, the tic and toc instructions in MATLAB 6.5 are the tools to assess the computational time utilized in each method. Numerical simulation in this aspect is conducted by using, the 512-MHz RAM and the 2.80-GHz Pentium(R)-4 CPU.

4.1 AML Estimator

To demonstrate the impact of the proposed estimator, we customarily employ the ULA with half-wavelength separation to receive two equi-powered QPSK (*q*uaternary *p*hase *s*hift *k*eying) signals whose strength are controllable with respect to noise variance by

$$\mathrm{SNR} \triangleq 10 \log \left(\frac{\sigma_s^2}{\sigma_n^2} \right). \tag{4.1}$$

Significant parameters are set up, unless otherwise a variation on the parameter of interest will be specified individually in each figure, as the table 4.1. In all situations, assume that the path power in each cluster is fixed as $\rho_{n_S} = 1 \; ; \forall n_S$. The pseudo random number satisfied by the standard Laplacian PDF $f_{\mathrm{L}}(\delta_\phi | 0, 1)$ can be, in practice, modified from [19]

$$\delta_{\phi_{\mathrm{L}}} = \frac{1}{\sqrt{2}} \ln \left(\frac{\delta_{\phi_{\mathrm{U}}}}{\acute{\delta}_{\phi_{\mathrm{U}}}} \right) \tag{4.2}$$

with any two independent uniform distributions $\delta_{\phi_{\mathrm{U}}} \sim \mathcal{U}[0, 1]$ and $\acute{\delta}_{\phi_{\mathrm{U}}} \sim \mathcal{U}[0, 1]$. Our empirical standard deviation (RMSE) is the square root of averaging the error square from a large number of independent runs (N_R).

Optimally, the exact ML [9] require joint $3N_S + 1$ dimension search. With an insignificant modification, we compute $2N_S$-dimensional *w*eighted *l*east *s*quares (WLS) [9] in the same sense as [35] from

$$\hat{\boldsymbol{\vartheta}}_{\mathrm{WLS}} = \arg \min_{\boldsymbol{\vartheta}_\omega} \hat{\boldsymbol{\xi}}_x^{\mathsf{H}} \hat{\boldsymbol{\Psi}}_{xx}^{-\frac{1}{2}} \boldsymbol{\Pi}^{\perp}_{\mathcal{S}_{\mathcal{R}}\left(\boldsymbol{\Omega}(\boldsymbol{\vartheta}_\omega) \hat{\boldsymbol{\Psi}}_{xx}^{-\frac{1}{2}}\right)} \hat{\boldsymbol{\Psi}}_{xx}^{-\frac{1}{2}} \hat{\boldsymbol{\xi}}_x. \tag{4.3}$$

$\phi_\circ$	$\sigma_{\phi_\circ}$	SNR	N_E	N_P	N_R
$0°, 10°\&12°$	$5°$	3&10	8	50&100	1,000

Table 4.1 Significant parameters in the numerical simulations of AML estimator.

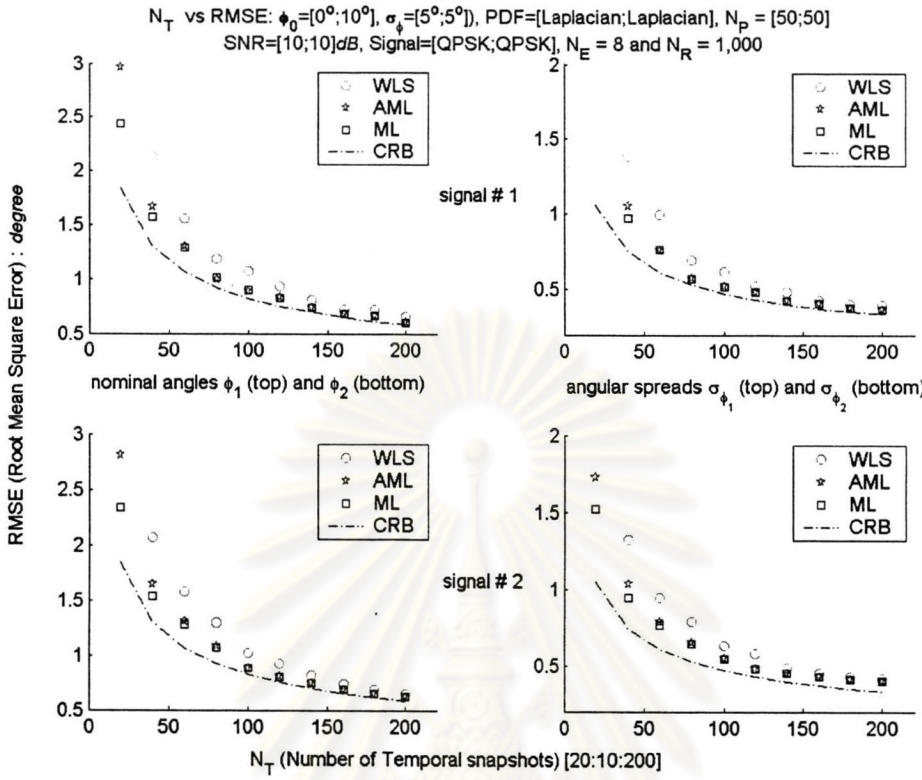

Figure 4.1 AML estimator in Laplacian angle deviations : empirical and theoretical standard deviations of the estimate errors as a function of number of snapshots N_T.

Including the estimation of spatial coherence parameter which is not of interest herein, we apply the *r*edundancy *a*veraging *c*ovariance *m*atching (RACM) [40], needing jointly $2N_S$-dimensional optimization, to estimate only the nominal angles. Since it is miss-modlled as exponential coherence model, the RACM is not desired for joint estimation of nominal angles and angular spreads. Although RACM requires, in addition, preliminary computation of all $N_E - 1$ Toepliz lags, our large-sample ML estimator is roughly comparable to WLS and RACM since both AML and WLS need $\hat{\boldsymbol{\Psi}}_{xx}^{-1}$ beforehand.

4.1.1 AML Performance

By inspecting Fig. 4.1, we investigate the effect of number of snapshot N_T in the situation where angle deviation is in most realistic, *i.e.*, Laplacian distribution [14]. When increasing the number of snapshots, the AML estimate is gradually comparable to that available from ML. Its RMSE is identical to ML in large sample, *i.e.*, around $N_T = 80$, and eventually attains the CRB. Note that in the aspect of rate converging to ML performance the AML estimator achieves CRB more rapid than the WLS. This is

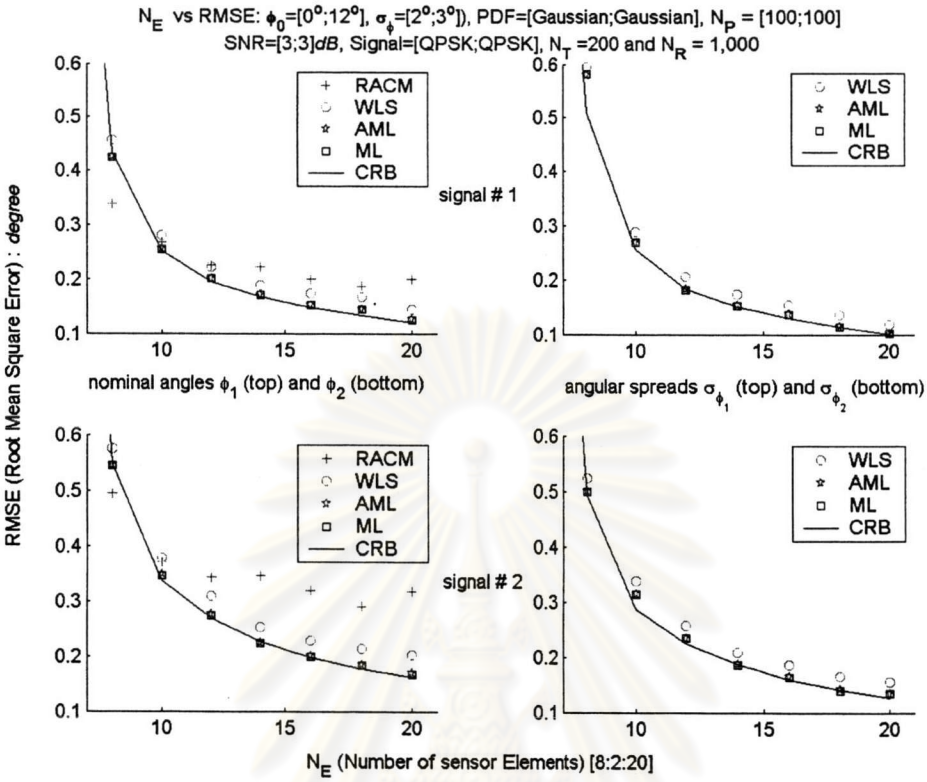

Figure 4.2 AML estimator in Gaussian angle deviations : empirical and theoretical standard deviations of the errors due to estimating the nominal angle ϕ as a function of number of sensor elements N_E.

because its exact weight matrix of WLS is replaced with the consistent one.

Next we shall investigate the error effect due to any number of sensor elements in Fig. 4.2. Setting up all parameters according to [40, Fig. 4], one can argue that the RACM does not absolutely achieve the CRB. This belongs to the fact that its coherence parameter is assigned, in whatever angle deviation, to be exponential function which can not coincides with the Gaussian spatial fading correlation aligned in the first sub-diagonal of $\boldsymbol{B}(\sigma_\phi)$. As kept $N_T = 200$, such asymptotic region allows the AML to be identical to ML whereas the WLS to be not yet.

Fig. 4.3 keeps $N_T = 100$ and varies SNR from 0 to 10 dB. As expected, higher SNR results in lower CRB. In this situation, the AML rather behaves well as the exact ML. It does not achieve the CRB because of invoking $N_T = 100$.

For angular spread viewpoint, in Fig. 4.4 the number of snapshot is set up to hold a rather asymptotic region. As expected earlier, the RACM obviously deviates from the CRB, particularly in large quantities of angular spread. One can see that the AML still, fortunately, outperforms the WLS at large angular spread. It is also equivalent to the

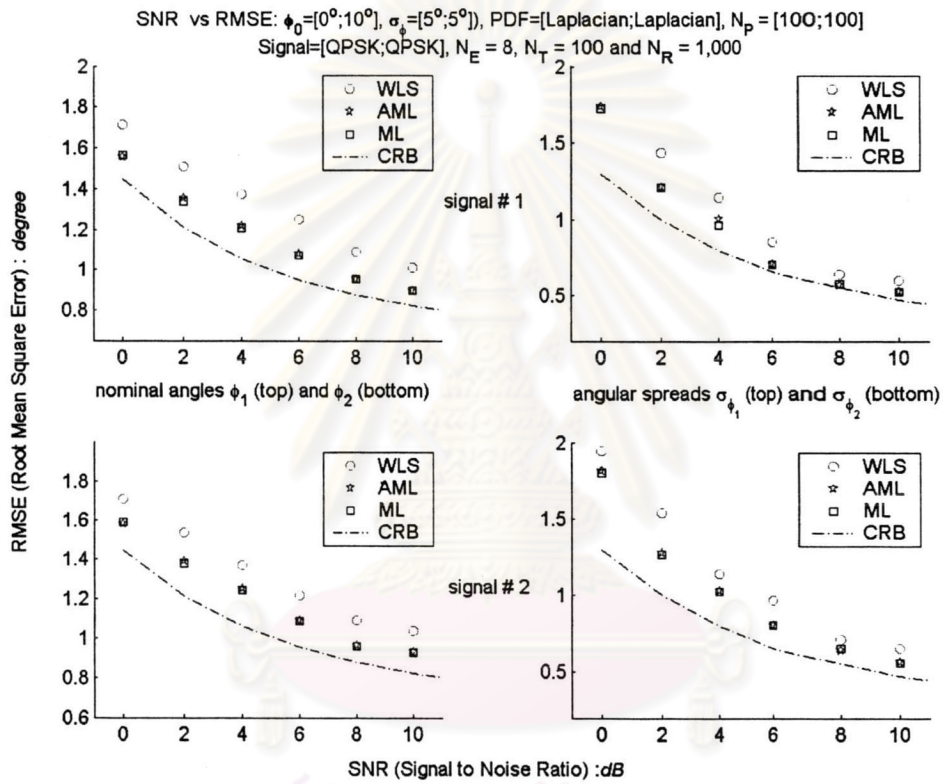

Figure 4.3 AML estimator in Laplacian angle deviations : empirical and theoretical standard deviations of the errors due to estimating the nominal angle ϕ as a function of number of SNR.

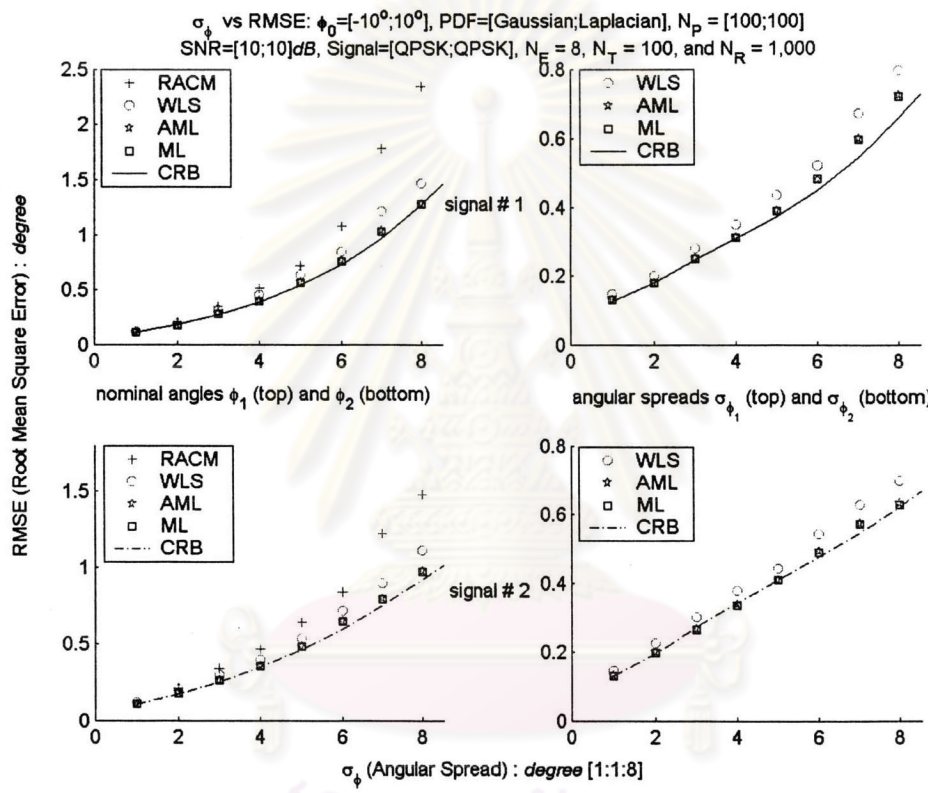

Figure 4.4 AML estimator in Gaussian and Laplacian angle deviations : empirical and theoretical standard deviations of the estimate errors as a function of angular spread σ_ϕ in $\boldsymbol{\sigma}_\phi = [\sigma_\phi \quad \sigma_\phi]^\mathsf{T}$.

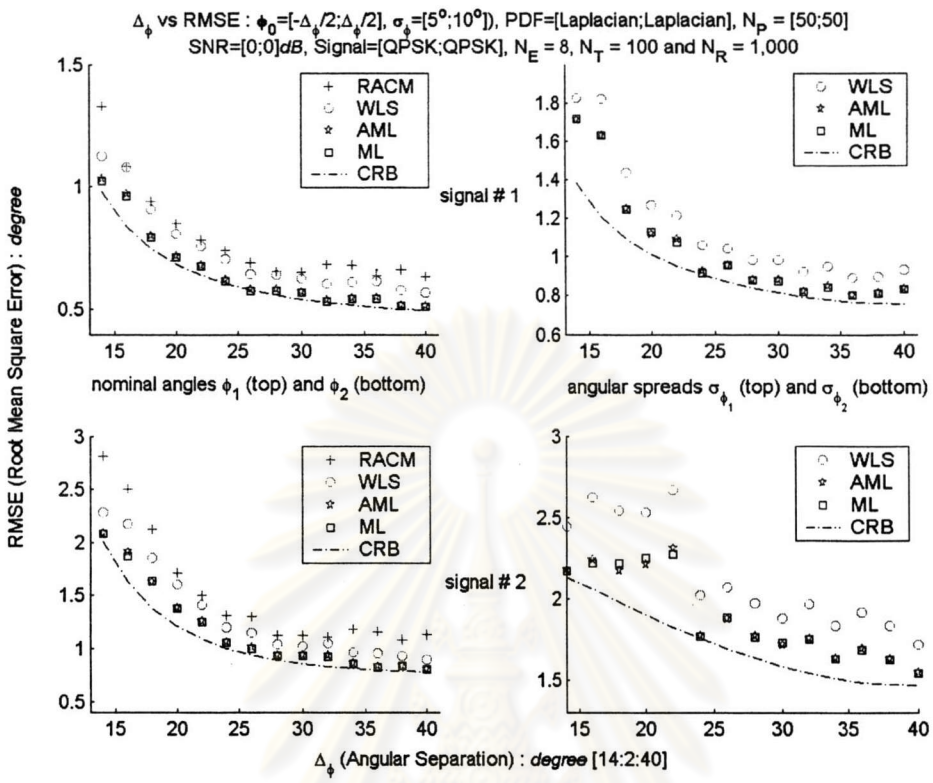

Figure 4.5 AML estimator in Gaussian and Laplacian angle deviations : empirical and theoretical standard deviations of the errors due to estimating the nominal angle ϕ as a function of angular separation $\Delta_\phi \triangleq |\phi_2 - \phi_1|$, where nominal angles are varied as $\phi_1 = -\frac{1}{2}\Delta_\phi$ and $\phi_2 = \frac{1}{2}\Delta_\phi$.

ML which attains the CRB quit well. This figure demonstrates a prominent superiors of AML estimator whose performance is satisfactorily comparable to that of the exact ML without any loss of asymptotic performance.

Finally, Fig. 4.5 is conducted to investigate the situation where each nominal direction of two signals is translated symmetrically with respect to array broadside. As already expected, the smaller the angular separation, the more the spatial correlation between both signals. This effect can be observed in high CRB standard deviation for small Δ_ϕ. Since small quantities of angular separation yields difficulty in angular spread estimation, the calculated RMSEs thus reflect more fluctuations, especially in the second signal whose angular spread is rather large ($\sigma_{\phi_2} = 10°$).

4.1.2 AML Complexity

Fig. 4.6 plots the ratio of computational times between the exact ML estimator and the WLS/AML. As being higher in non-asymptotic performance than the WLS estimator,

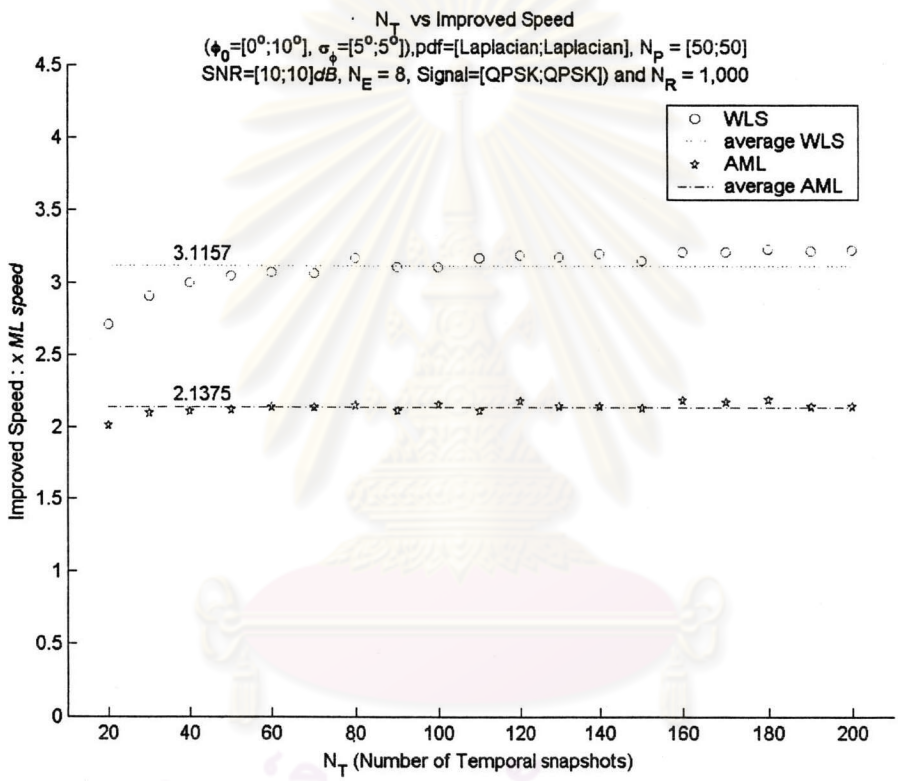

Figure 4.6 Computational complexity with respect to the exact ML estimator as a function of number of snapshots N_T.

ϕ_o	σ_{ϕ_o}	σ_γ^2	SNR	N_P	N_E
0°	5°	0.01	10	100	8

Table 4.2 Significant parameters in the numerical simulations of improved WLS estimators.

the AML is shown under the situation of Fig. 4.1 that its computational speed with respect to the exact ML is more worse than that required by the WLS approximately one time.

4.2 Toeplitz Constraint Applications

4.2.1 Improved WLS Estimators

In addition to verification of the lemma 3, the following simulations also demonstrate the impact of two proposed improvements. Significant parameters are set up, unless otherwise a variation on the parameter of interest will be specified individually in each figure, as the table 4.2:

By inspecting the single source case in Fig. 4.7, 4.8 and 4.9, all WLS-based estimators asymptotically achieve the corresponding CRBs, *i.e.*, uniform, Gaussian and Laplacian CRBs, respectively. It is noteworthy that the WLS estimators employing the Toeplitz-constrained weights, such as RA and WCM covariance estimates, outperform the ordinary WLS, particularly in small and moderate numbers of temporal snapshots. Furthermore, both converge to the CRB at hand more rapid than the ordinary WLS. This is due to the fact that, in each improvement, the consistent weight matrix has been forced beforehand to be of Toeplitz structure accounting for a property of optimal weight. For more insight into the improved weight reflections, the WCM-WLS is better than the RA-WLS, especially in small number of temporal snapshots. This superiority agrees well with the lemma 3 which can be infered that the WCM weight estimate will provide error less than that given from RA weight estimation.

4.2.2 Improved AML Estimator

4.2.2.1 Performance of the Improved AML

For all situations, we assume that the path power in each cluster is normalized as $\rho \triangleq N_P\sigma_\gamma^2 = 1$. Pseudo random number satisfied by the standard Laplacian PDF can be modified from [19]. Significant parameters are set up, unless otherwise a variation on the parameter of interest will be specified individually in each figure, as the table 4.3.

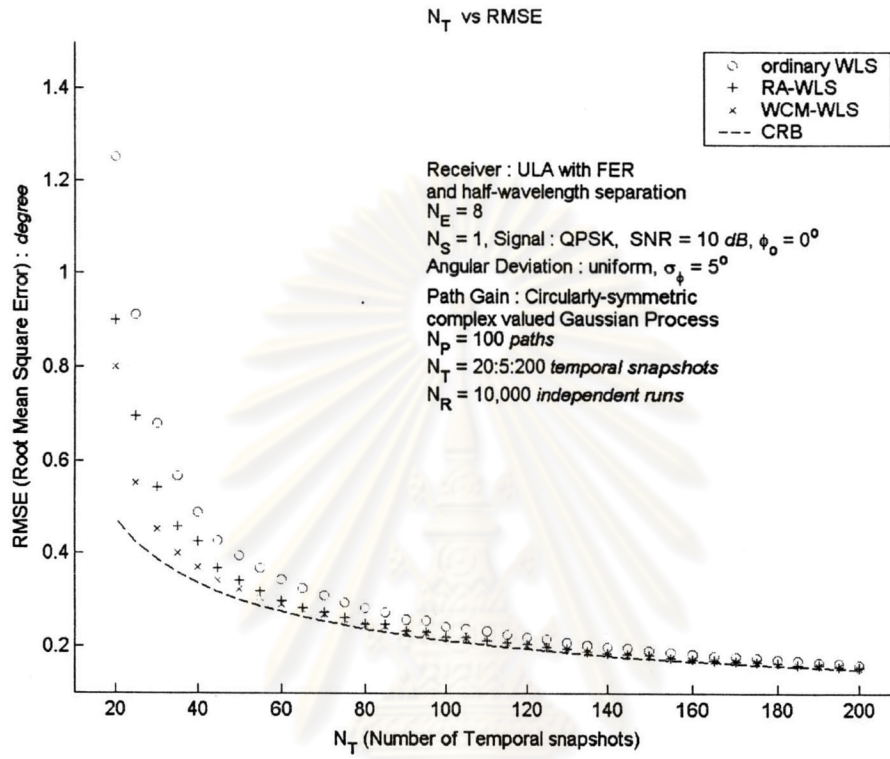

Figure 4.7 Improved WLS estimators in uniform angle deviation: empirical and theoretical standard deviations of the errors due to estimating the nominal angle ϕ as a function of the number of temporal snapshots N_T.

ϕ_o	σ_{ϕ_o}	SNR	N_E	N_P	N_R
0°	5°	10	8	100	10,000

Table 4.3 Significant parameters in the numerical simulations of improved AML estimator.

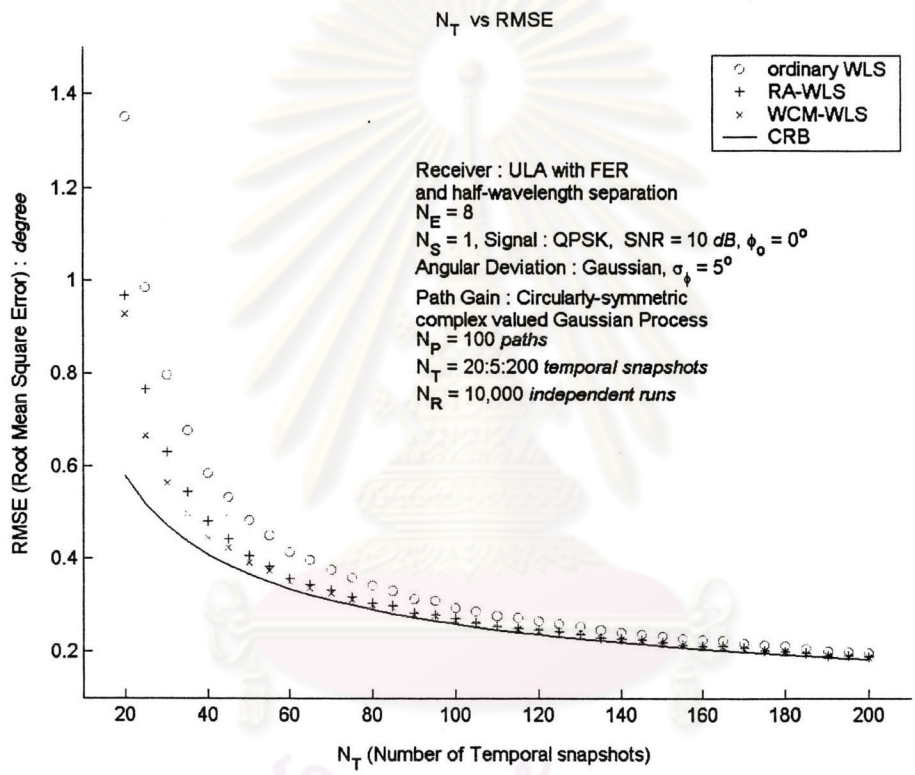

Figure 4.8 Improved WLS estimators in Gaussian angle deviation: empirical and theoretical standard deviations of the errors due to estimating the nominal angle ϕ as a function of the number of temporal snapshots N_T.

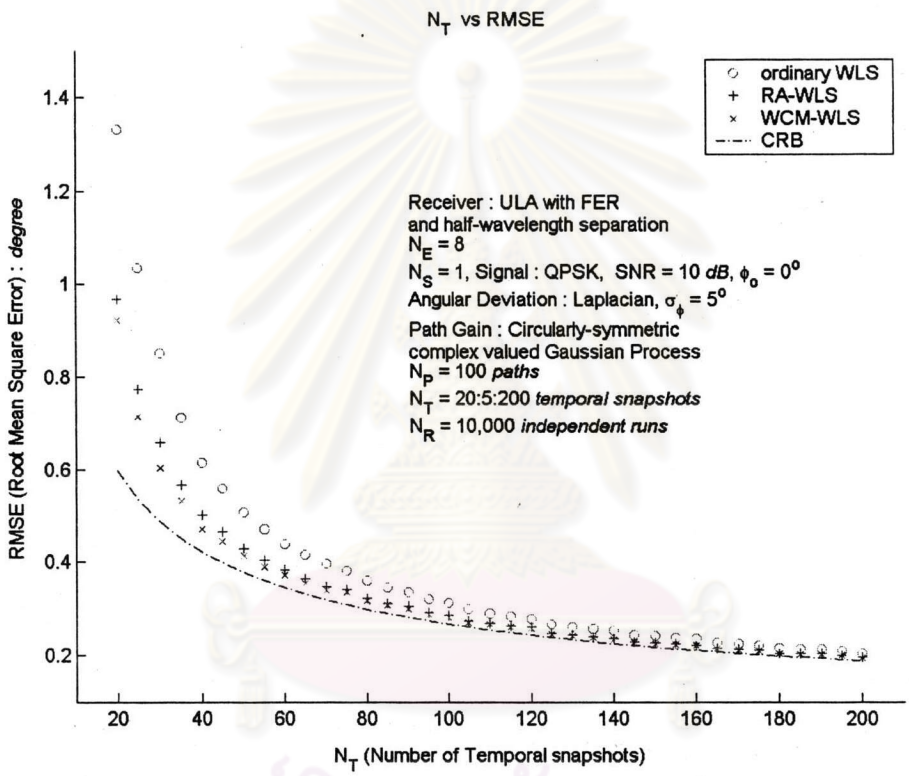

Figure 4.9 Improved WLS estimators in in Laplacian angle deviation: empirical and theoretical standard deviations of the errors due to estimating the nominal angle ϕ as a function of the number of temporal snapshots N_T.

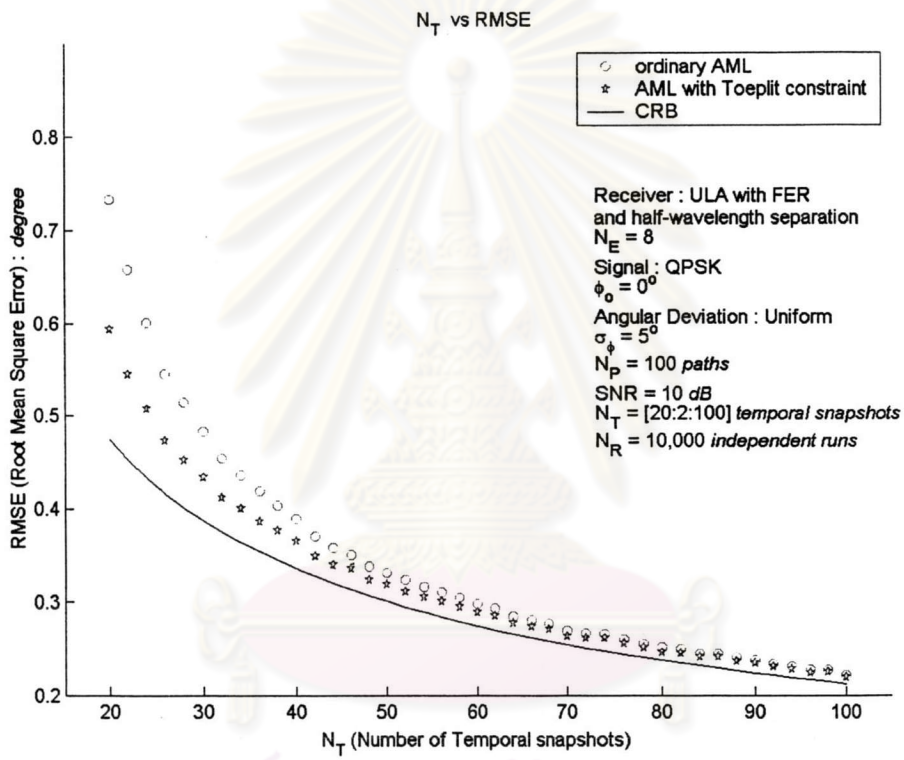

Figure 4.10 Improved AML estimator in uniform angle deviation: empirical and theoretical standard deviations of the estimate errors as a function of the number of snapshots N_T.

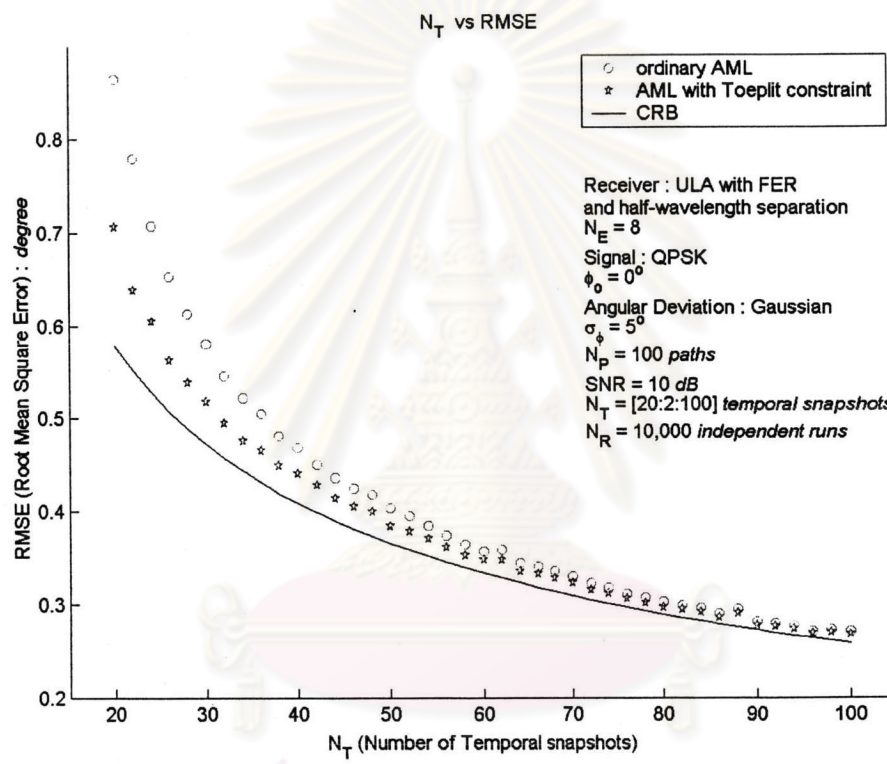

Figure 4.11 Improved AML estimator in Gaussian angle deviation: empirical and theoretical standard deviations of the estimate errors as a function of the number of snapshots N_T.

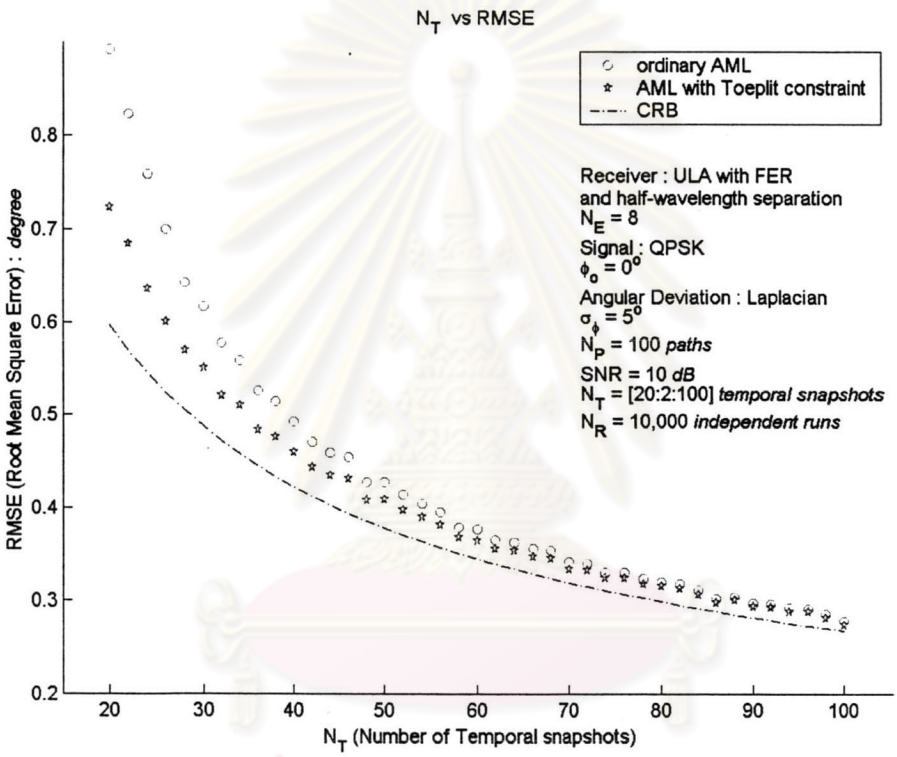

Figure 4.12 Improved AML estimator in Laplacian angle deviation: empirical and theoretical standard deviations of the estimate errors as a function of the number of snapshots N_T.

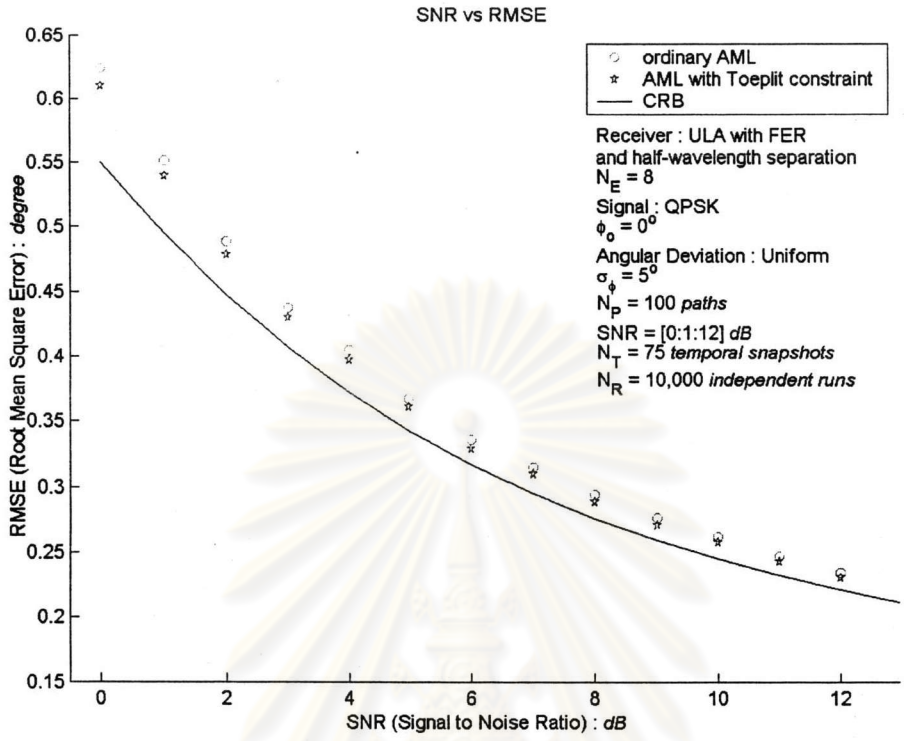

Figure 4.13 Improved AML estimator in Uniform angle deviation: empirical and theoretical standard deviations of the estimate errors as a function of SNR.

In Fig. 4.10, 4.11 and 4.12, we plot empirical and theoretical standard deviations of the errors due to estimating the nominal angle ϕ as a function of number of snapshots N_T. Both AML-based estimates attain each Cramér-Rao bound (CRB) at hand asymptotically, *i.e.*, as the number of temporal snapshot tends to be infinity. Since the AML with Toeplitz constraint is more accurate than one without this knowledge, the RMSE in this way is thus lower than such ordinary AML. This can be observed in all angular PDFs.

Fig. 4.13, 4.14 and 4.15 are the plots of empirical and theoretical standard deviations of the errors due to estimating the nominal angle ϕ as a function of SNR. In all angle deviation models, the AML with Toeplitz constraint outperforms the ordinary AML estimator. It can be observed evidently in small SNR. Note that both AML-based estimators do not achieve the CRB. The cause of this is that as mentioned earlier, the AML will attain the CRB when the number of temporal snapshots tends to infinity (see Fig. 4.10, 4.11 and 4.12). Since $N_T = 75$ in Fig. 4.13, 4.14 and 4.15, there must be unattainable gaps.

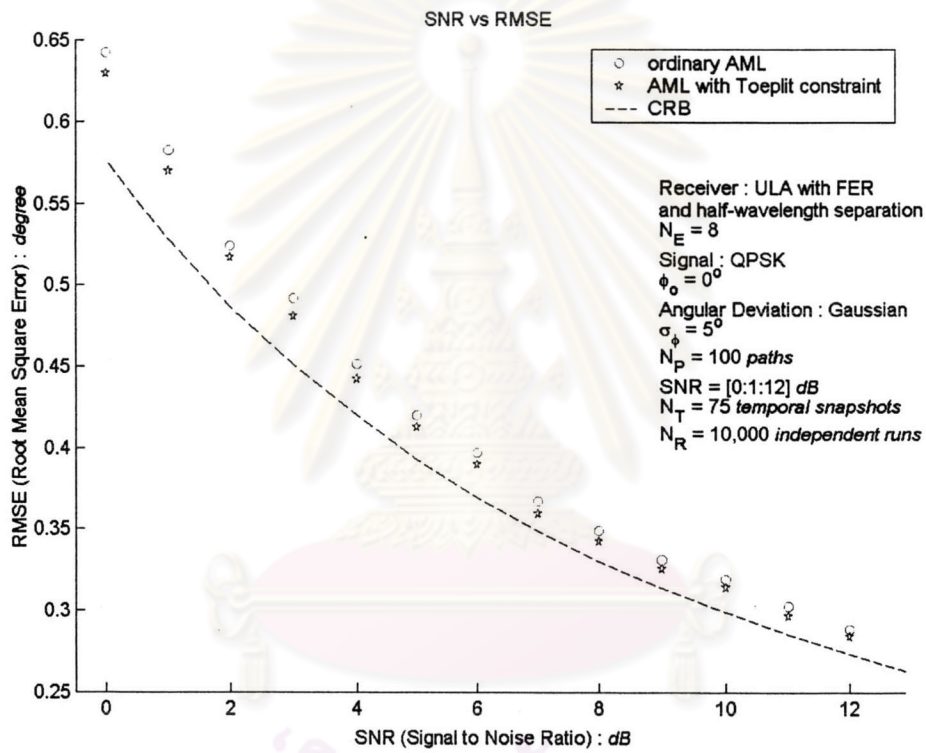

Figure 4.14 Improved AML estimator in Gaussian angle deviation: empirical and theoretical standard deviations of the estimate errors as a function of SNR.

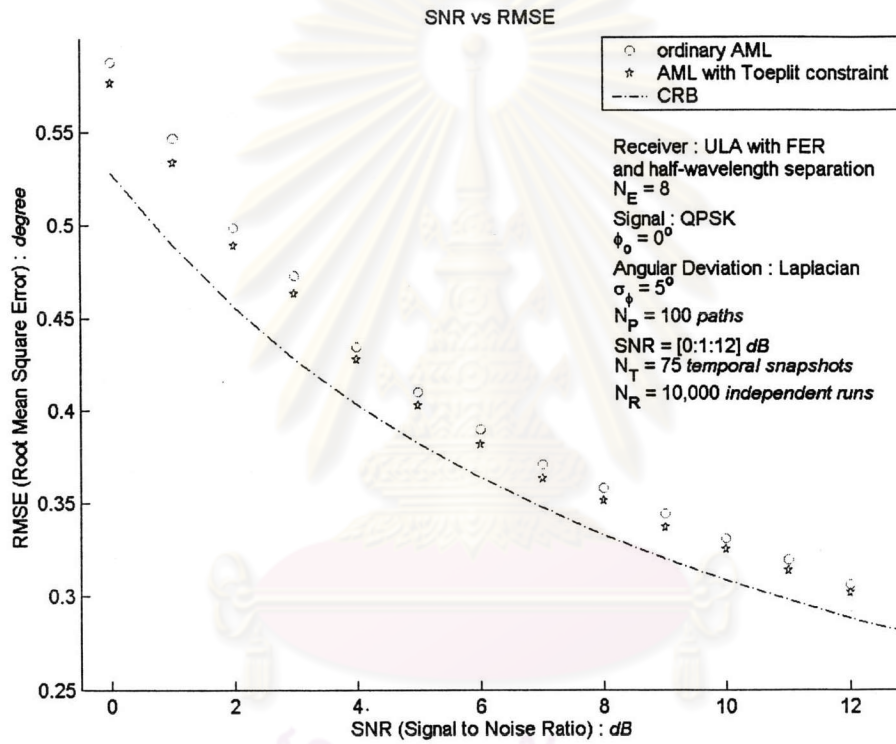

Figure 4.15 Improved AML estimator in Laplacian angle deviation: empirical and theoretical standard deviations of the estimate errors as a function of SNR.

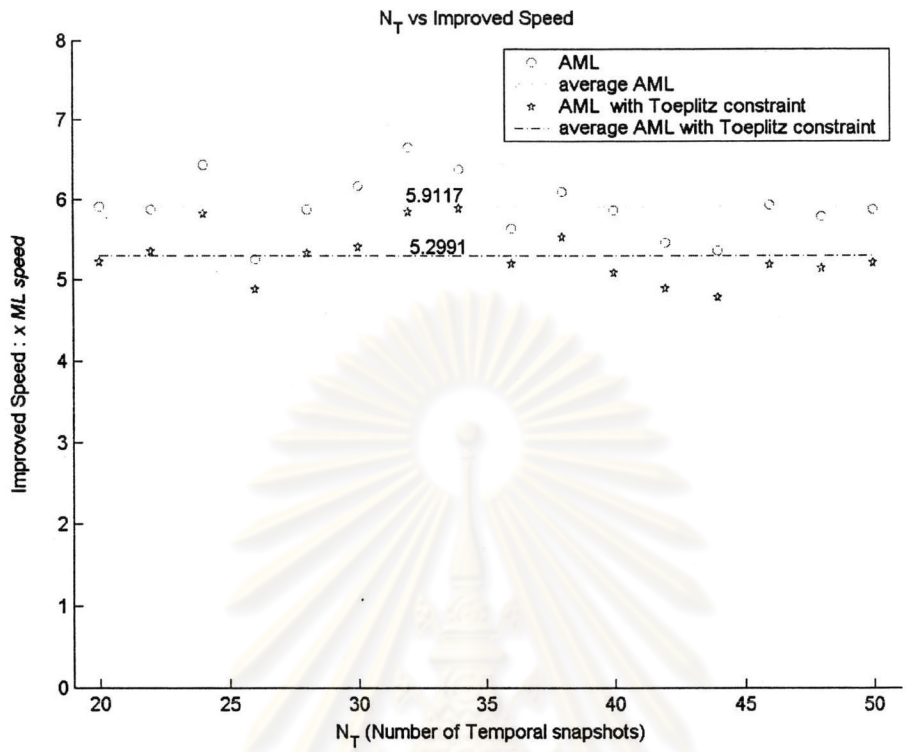

Figure 4.16 Improved AML estimator in uniform angle deviation: computational speed with respect to the exact ML estimator as a function of the number of snapshots N_T.

4.2.2.2 Complexity of the Improved AML

Fig. 4.16, 4.17 and 4.18, are the plots of computational beneficence of the AML-base algorithms with respect to the exact ML estimator. In these three figures, the AML with Toeplitz constraint requires more slightly calculation than the ordinary AML. This is the operation of forcing the sample covariance matrix to be Toeplitz. However, this addition calculation is small with respect to the exact ML, that is, the calculation difference between both methods is less than one time of that utilized in the exact ML estimator.

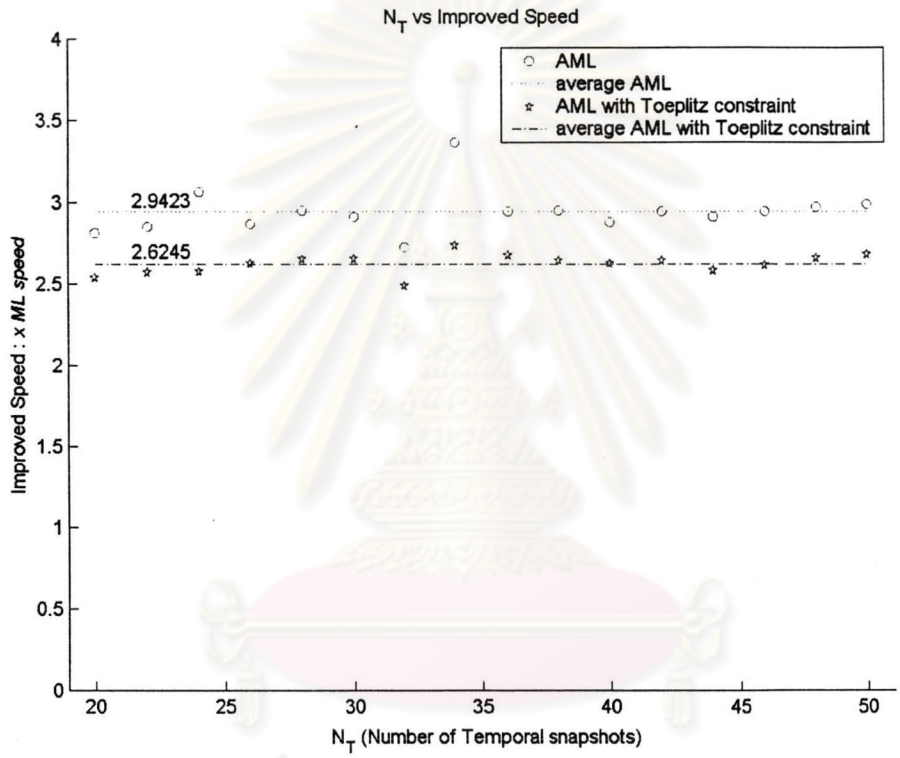

Figure 4.17 Improved AML estimator in Gaussian angle deviation: computational speed with respect to the exact ML estimator as a function of the number of snapshots N_T.

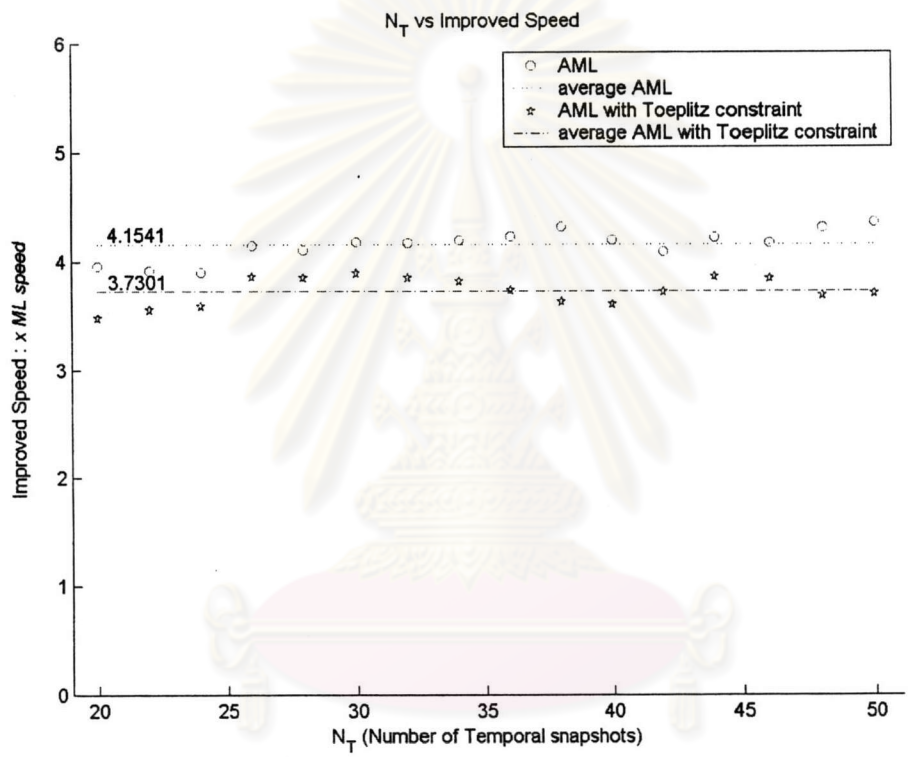

Figure 4.18 Improved AML estimator in Laplacian angle deviation: computational speed with respect to the exact ML estimator as a function of the number of snapshots N_T.